Integrated ternary artificial nacre via synergistic toughening of reduced graphene oxide/double-walled carbon nanotubes/poly(vinyl alcohol)

2016 Mater. Res. Express 3 075002

(http://iopscience.iop.org/2053-1591/3/7/075002)

Materials Research Express

PAPER

Integrated ternary artificial nacre via synergistic toughening of reduced graphene oxide/double-walled carbon nanotubes/poly (vinyl alcohol)

RECEIVED
17 May 2016

REVISED
31 May 2016

ACCEPTED FOR PUBLICATION
9 June 2016

PUBLISHED
29 June 2016

Shanshan Gong[1], **Mengxi Wu**[1], **Lei Jiang**[1] **and Qunfeng Cheng**[1,2]

[1] Key Laboratory of Bio-inspired Smart Interfacial Science and Technology of Ministry of Education, School of Chemistry and Environment, BeiHang University, Beijing, 100191, People's Republic of China

[2] State Key Laboratory for Modification of Chemical Fibers and Polymer Materials, Donghua University, Shanghai 201620, People's Republic of China

E-mail: cheng@buaa.edu.cn

Keywords: nacre, bioinspired, graphene oxide, nanocomposites, synergistic toughening

Abstract

The synergistic toughening effect of building blocks and interface interaction exists in natural materials, such as nacre. Herein, inspired by one-dimensional (1D) nanofibrillar chitin and two-dimensional (2D) calcium carbonate platelets of natural nacre, we have fabricated integrated strong and tough ternary bio-inspired nanocomposites (artificial nacre) successfully via the synergistic effect of 2D reduced graphene oxide (rGO) nanosheets and 1D double-walled carbon nanotubes (DWNTs) and hydrogen bonding cross-linking with polyvinyl alcohol (PVA) matrix. Moreover, the crack mechanics model with crack deflection by 2D rGO nanosheets and crack bridging by 1D DWNTs and PVA chains induces resultant artificial nacre exhibiting excellent fatigue-resistance performance. These outstanding characteristics enable the ternary bioinspired nanocomposites have many promising potential applications, for instance, aerospace, flexible electronics devices and so forth. This synergistic toughening strategy also provides an effective way to assemble robust graphene-based nanocomposites.

Natural nacre, consisting of one-dimensional (1D) nanofibrillar chitin and two-dimensional (2D) calcium carbonate platelets simultaneously [1], possesses favorable mechanical properties with integrated strength and toughness, which are attributed to the synergy of rational interface and admirable hierarchical micro/nanoscale layered structure [1, 2]. In recent years, scientists have utilized this mechanism of structural design to assemble biomimetic composites with interface bonding force and inorganic fillers [3]. The interfaces are designed via various cross-links [4], including hydrogen bonding of graphene oxide (GO)-poly(methyl methacrylate) PMMA [5] and reduced GO (rGO)-silk fibroin (SF) [6] films, ionic cross-linking of GO-Ca^{2+} [7] and GO-Mg^{2+} [7] papers, covalent cross-linked GO-Borate [8], rGO-polydopamine (PDA) [9] and PDA-capped GO-polyetherimide (PEI) [10] composites and π–π conjugated nanocomposite cross-linked by poly (acrylic acid-co-(4-acrylamidophenyl) boronic acid) (PAPB) [11].

Moreover, different inorganic additives with outstanding characteristics are used as building blocks [2, 12], for example, montmorillonite (MMT) [13], alumina flakes [14], disulphides [12], double hydroxide platelets [15], carbon-based materials [3, 16] and other additives. Kakisawa's group fabricated nacre-like composites through a new hybrid metallurgical technique hot-press assisted slip casting with alumina flakes as building blocks [17]. Based on molybdenum disulfide (MoS_2) nanosheets, Liu *et al* [18] prepared the layered polymeric nanocomposites by coordinating with bivalent copper ions, tremendously improving the mechanical properties of the MoS_2 paper. Carbon-based building blocks, for instance, GO [19], carbon nanotubes (CNT) [16, 20] and graphdiyne [16], have attracted great attention for promising device applications [19, 20], which is attributed to their extraordinary performance, especially mechanical and electrical features [16, 19, 20]. GO, a typical 2D inorganic filler [21], was applied to fabricate rGO-polyvinyl alcohol (PVA) composite film with ultrahigh

mechanical properties (the tensile strength reaches to 188.9 MPa, while the toughness is 2.52 MJ m^{-3}), high electrical conductivity (5265 s m^{-1}) and excellent biocompatibility [22].

On the other hand, the synergistic effect of building blocks plays a very important role in enhancing the properties of biological nanocomposites [2, 3, 23]. In previous reports, Liao *et al* [24] and Liu *et al* [25] both mentioned the synergistic reinforcing effect from the combination of 2D GO and 1D CNT in GO-CNT-PVA [24] and (functionalized multi-walled CNT) fCNT-rGO-PVA composites [25], which were filled with low building blocks content (only less than 1 wt%), showing relatively poor mechanical properties. The appropriate weight ratios of building blocks should be regulated to improve the mechanical properties. Our previous works, the synergistic toughening effect was demonstrated in bioinspired nanocomposites with relatively high mass fraction of fillers, for example, synergy of 2D building blocks for integrated strong and tough ternary rGO-MoS_2-thermoplastic polyurethanes (TPU) [26] with 90 wt% inorganic fillers and rGO-MMT-PVA [27] with both GO and MMT content of 90.6 wt%, the combination of 2D and 1D building blocks for high-performance artificial nacre of the nanofibrillar cellulose (NFC)-MMT-PVA [28] with 70 wt% additives and rGO-double-walled carbon nanotubes (DWNTs)-10,12-pentacosadiyn-1-ol (PCDO) [29] with inorganic content of 98 wt%. Although some of remarkable mechanical properties, such as strength and toughness, have been achieved, however, it is still a great challenge to build integrated graphene-based nanocomposites by synergistic toughening effect of the building blocks.

Herein, inspired by natural nacre [2, 30], we explore an efficient strategy for assembling high-performance artificial nacre through synergistic toughening effect of 2D rGO nanosheets and 1D DWNTs with matrix of PVA. The tensile strength and toughness of the resultant ternary bio-inspired nanocomposites are as high as 375.8 ± 9.3 MPa and 11.3 ± 0.01 MJ m^{-3}, which are 1.9 and 4.3 times higher than natural nacre (tensile strength of 200 MPa and toughness of 2.6 MJ m^{-3} [2]), respectively. Moreover, this ternary bioinspired nanocomposites also exhibit superior fatigue-resistance property, which enable our new materials for use in many fields, for example, aerospace, flexible electronics device and other fields. Furthermore, this synergistic toughening strategy of building blocks along with interface interaction provides a new way to construct graphene-based bioinspired nanocomposites with superior mechanical performance.

The GO nanosheets were prepared via modified Hummers' method. The tensile strength and toughness of assembled DWNTs films were 33.9 ± 2.6 MPa and 1.5 ± 0.3 MJ m^{-3}, respectively, as shown in supplementary information in figure S1. Four different weight ratios of GO to PVA (100:0, 70:30, 50:50, 30:70) were chosen to fabricate the binary GO-PVA nanocomposites by evaporation assembly approach. The tensile strength and toughness of binary GO-PVA nanocomposites reached maximum values when the weight ratio of GO to PVA was 50:50, as shown in figure S2. Thus, the ternary GO-DWNTs-PVA nanocomposites were fabricated based on binary GO-PVA (50:50) nanocomposites in the following experiments.

The fabrication process of the ternary bio-inspired nanocomposites was shown in figure 1(a), which is similar to our previous reports [28, 29]. In this process, four kinds of ternary GO-DWNTs-PVA artificial nacre were obtained, including GO-DWNTs-PVA-I (GO:DWNTs = 400:2), GO-DWNTs-PVA-II (GO:DWNTs = 400:4), GO-DWNTs-PVA-III (GO:DWNTs = 400:5) and GO-DWNTs-PVA-IV (GO:DWNTs = 400:11), respectively. Finally, the final ternary bioinspired rGO-DWNTs-PVA nanocomposites (figure 1(b)) were achieved after chemical reduction by 57 wt% hydroiodic acid (HI), and the corresponding digital photographs was shown in figure 1(b). The cross-section fracture morphologies with different magnification were shown in figure 1(c). Transmission electron microscope of the rGO-DWNTs-PVA-II was a direct evidence to illustrate that DWNTs uniformly disperse between rGO layers, as shown in figure S3. Moreover, the corresponding DWNTs-PVA-I (2:400), DWNTs-PVA-II (4:400), DWNTs-PVA-III (5:400) and DWNTs-PVA-IV (11:400) nanocomposites were also prepared.

The results of x-ray diffraction exhibit the interlayer distance of pure GO film, binary GO-PVA (50:50), ternary GO-DWNTs-PVA-II nanocomposites and the corresponding films after chemical reduction, which is shown in figure S4. The corresponding data are summarized in table S1. It is clearly that the peak position changes with the successive intercalation of PVA and DWNTs, especially after chemical reduction by HI. The interlayer distance (d-spacing) increases from 3.70 Å ($2\theta = 20.06$) for the pure rGO film to 4.33 Å ($2\theta = 20.48$) for the binary rGO-PVA nanocomposites (the GO content is about 50%), and continually increasing to 4.38 Å ($2\theta = 20.28$) for the ternary rGO-DWNTs-PVA-II artificial nacre. The above evidence indicates that both the polymer chains and 1D building block are inserted into the GO nanosheets successfully.

The typical tensile stress-strain curves of pure GO film (Curve 1), rGO film (Curve 2), binary GO-PVA (Curve 3) nanocomposites, binary rGO-PVA nanocomposites (Curve 4), ternary GO-DWNTs-PVA-II (Curve 5) and rGO-DWNTs-PVA-II (Curve 6) nanocomposites are compared in figure 2(a). The tensile strength of pure GO film reaches to 87.5 ± 10.3 MPa, while the toughness is 0.3 ± 0.02 MJ m^{-3}, respectively. After incorporating with an equal amount of PVA, the optimal tensile strength and toughness of binary GO-PVA nanocomposites are 240.4 ± 30.8 MPa and 2.0 ± 0.5 MJ m^{-3}, respectively, which is higher than natural nacre [2], as shown in figure S2. After chemical reduction with HI, most of oxygen-containing functional groups were

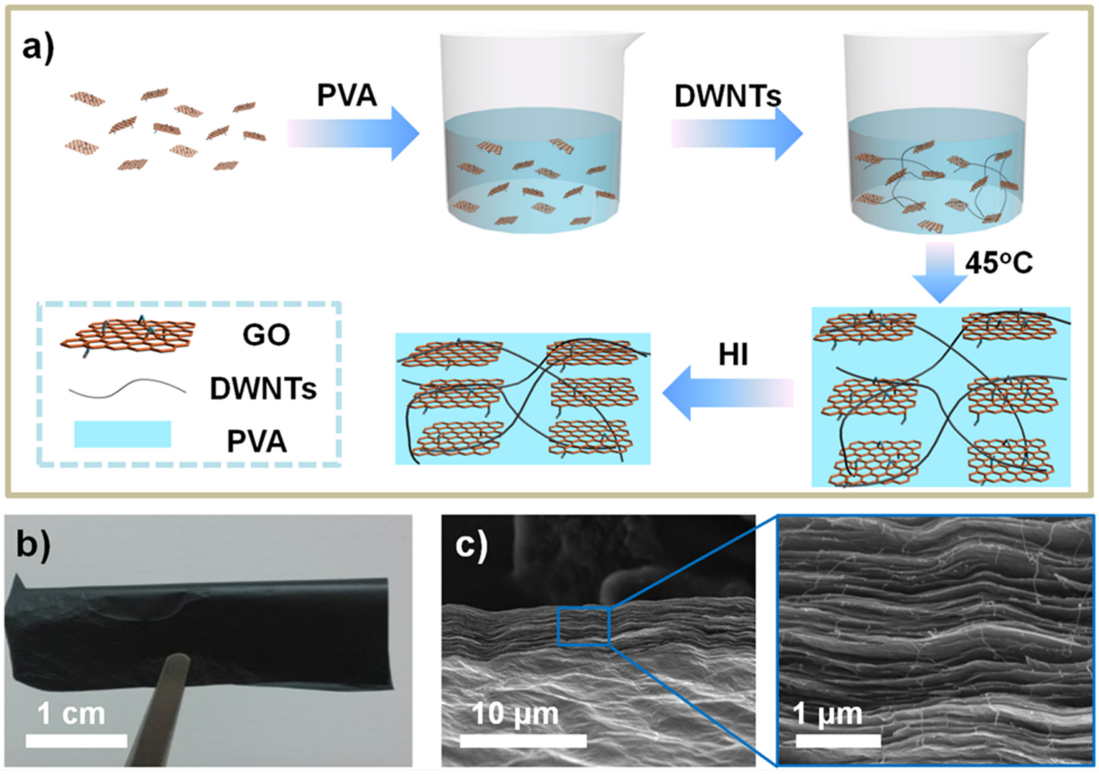

Figure 1. Illustration of the preparation process of the ternary artificial nacre. (a) The ternary GO-DWNTs-PVA film was fabricated via evaporation-induced self-assembly technique, and the bioinspired rGO-DWNTs-PVA nanocomposites were obtained through chemically reduced by 57 wt% HI. (b) Digital photograph of the ternary rGO-DWNTs-PVA nanocomposites. (c) SEM images of cross-section morphology of the bioinspired rGO-DWNTs-PVA nanocomposites.

eliminated [31]. Meanwhile, the laminated structure of rGO-PVA nanocomposites would be further densified, reducing interlayer distance. Thus, the tensile strength of rGO-PVA nanocomposites increases to 291.4 ± 4.6 MPa, while the toughness reaches 5.9 ± 0.4 MJ m^{-3}. After introducing some amount of 1D building block (DWNTs) into the binary GO-PVA nanocomposites, the ternary GO-DWNTs-PVA-II possesses tensile strength of 323.0 ± 11.4 MPa and toughness of 5.8 ± 0.5 MJ m^{-3}, respectively, obviously superior to binary GO-PVA nanocomposites. The tensile strength of corresponding ternary rGO-DWNTs-PVA-II bioinspired nanocomposites dramatically improves to 375.8 ± 9.3 MPa, while the toughness is as high as 11.3 ± 0.01 MJ m^{-3}, which are 2.7 and 4.0 times higher than that of rGO film with tensile strength of 141.8 MPa and toughness of 2.8 MJ m^{-3}, respectively. The remarkable improvement of mechanical properties attributes the synergistic interactions of rGO and DWNTs and hydrogen bond cross-linking. The mechanical properties of rGO-PVA, rGO-DWNTs-PVA-I, rGO-DWNTs-PVA-II, rGO-DWNTs-PVA-III and rGO-DWNTs-PVA-IV nanocomposites with different DWNTs contents are compared in figures 2(b) and (c). The results show that the rGO-DWNTs-PVA-II nanocomposites achieve the maximum tensile strength of 384.2 MPa when DWNTs content is about 0.5 wt%, while the rGO-DWNTs-PVA-III nanocomposites achieve the maximum toughness of 19.3 MJ m^{-3} at 0.6 wt% DWNTs, which is far higher than other graphene-based nanocomposites. All of the details of microstructures and mechanical properties are listed in figure S6 and table S3 in supporting information. A small amount of DWNTs forms maximization of synergistic toughening effect together with rGO nanosheets, playing a very important role in improving the mechanical properties of ternary rGO-DWNTs-PVA nanocomposites. In addition, the mechanical properties of pure DWNTs film and four binary DWNTs-PVA nanocomposites with different DWNTs contents are listed in table S2.

The front view fracture morphologies of binary rGO-PVA and ternary bioinspired rGO-DWNTs-PVA-II nanocomposites are shown in figures 2(d) and (e). The results clearly show that the rGO-PVA nanocomposites exhibit a brittle fractured morphology after broken of hydrogen bonds, however, the curled rGO nanosheets and disorderly fracture morphology of the rGO-DWNTs-PVA-II nanocomposites reveal that the DWNTs and PVA chains are dragged out along the pulling direction, forming a large plastic deformation. A possible fracture mechanism for explaining synergistic toughening effect of 1D DWNTs and 2D rGO nanosheets is proposed in figure 2(f). In the early loading, adjacent rGO nanosheets start to slip, and then are bridged by the DWNTs and PVA molecular chains, preventing the further sliding between adjacent rGO nanosheets. Continue to stretching,

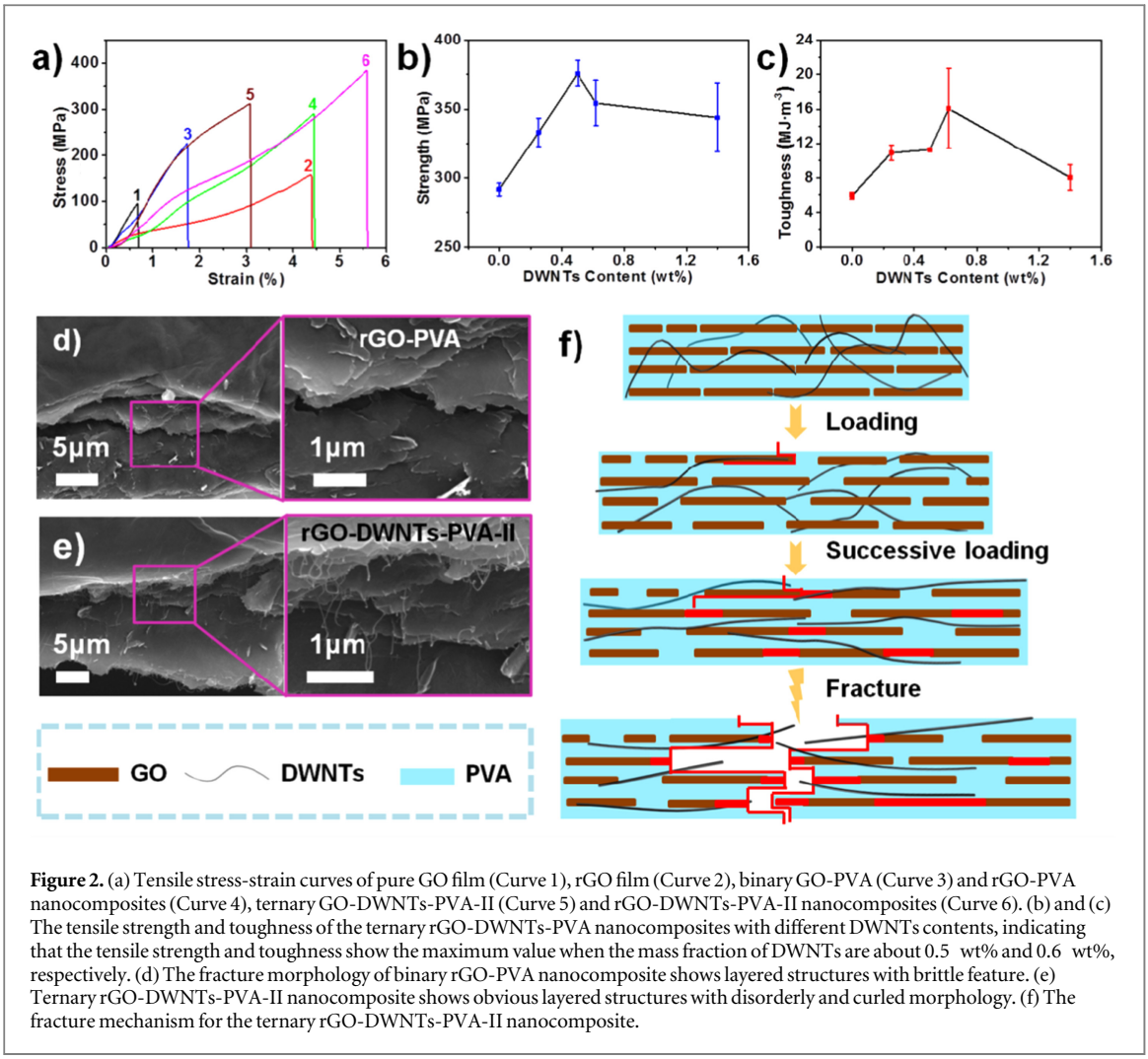

Figure 2. (a) Tensile stress-strain curves of pure GO film (Curve 1), rGO film (Curve 2), binary GO-PVA (Curve 3) and rGO-PVA nanocomposites (Curve 4), ternary GO-DWNTs-PVA-II (Curve 5) and rGO-DWNTs-PVA-II nanocomposites (Curve 6). (b) and (c) The tensile strength and toughness of the ternary rGO-DWNTs-PVA nanocomposites with different DWNTs contents, indicating that the tensile strength and toughness show the maximum value when the mass fraction of DWNTs are about 0.5 wt% and 0.6 wt%, respectively. (d) The fracture morphology of binary rGO-PVA nanocomposite shows layered structures with brittle feature. (e) Ternary rGO-DWNTs-PVA-II nanocomposite shows obvious layered structures with disorderly and curled morphology. (f) The fracture mechanism for the ternary rGO-DWNTs-PVA-II nanocomposite.

the coiled DWNTs and PVA chains, among the rGO nanosheets, are stretched along the drawing direction, dissipating much more energy. The hydrogen bonds between the PVA chains and rGO nanosheets are broken gradually. Further increasing the loading, the DWNTs are frictionally pulled out after the broken of π-conjugated interaction between rGO and DWNTs, which produces large plastic deformation. The external stress induces the ductile fracture morphology of the edge of the rGO nanosheets in the ternary rGO-DWNTs-PVA nanocomposites. The essence of synergistic toughening effect is to maximize the enhancement of 1D DWNTs and 2D rGO nanosheets in the fracture procedure, as shown in figure 2(f).

Owing to the synergistic toughening effect of 2D rGO nanosheets and 1D DWNTs with hydrogen bond cross-linking of PVA chains, the final ternary artificial nacre possesses integrated tensile strength and tough, superior to other various layered nanocomposites and natural nacre [2] (figure 3), including the ternary nanocomposites fabricated via synergistic effect from building blocks, such as MMT-NFC-PVA [28], rGO-MMT-PVA [27], rGO-MoS_2-TPU [26], rGO-DWNTs-PCDO [29], GO-CNT-PVA [24] and fCNT-rGO-PVA [25]. Meanwhile, the resultant ternary rGO-DWNTs-PVA-II nanocomposites also show higher mechanical properties than other graphene-based nanocomposites with cross-linked of divalent ions (Ca^{2+} [7], Mg^{2+} [7] and Cu^{2+} [32]), hydrogen bonding (GO-PMMA [5], rGO-PVA [22], GO-SF [33] and rGO-SF [6]), covalent cross-linking nanocomposites modified by glutaraldehyde (GA) [34], polyallylamine (PAA) [35], Borate [8], PEI [10], PCDO [36] and poly(dopamine) (PDA) [9], π–π conjugated interaction (rGO-PAPB) [11] and synergistic interfacial interactions (Borate-GO-PVA [37], GO-Fe^{3+}-tannic acid (TA) [38] and GO-polyimide (PI)-Mg^{2+} [39]), respectively. The details of mechanical properties for natural nacre, other graphene-based layered nanocomposites and our ternary artificial nacre are summarized in table S4.

The synergy, resulting from 2D rGO nanosheets and 1D DWNTs with assistance of PVA matrix, also induces artificial nacre possessing excellent fatigue resistance performance. The correlation parameters are set in accordance with previous works [29]. The curves of maximum tensile stress (S) versus number of cycles to failure (N) for pure GO film, rGO film, the binary rGO-PVA and ternary rGO-DWNTs-PVA-II nanocomposites are shown in figure 4 and the details of corresponding stress-strain curves are shown in figure S5. For the ternary

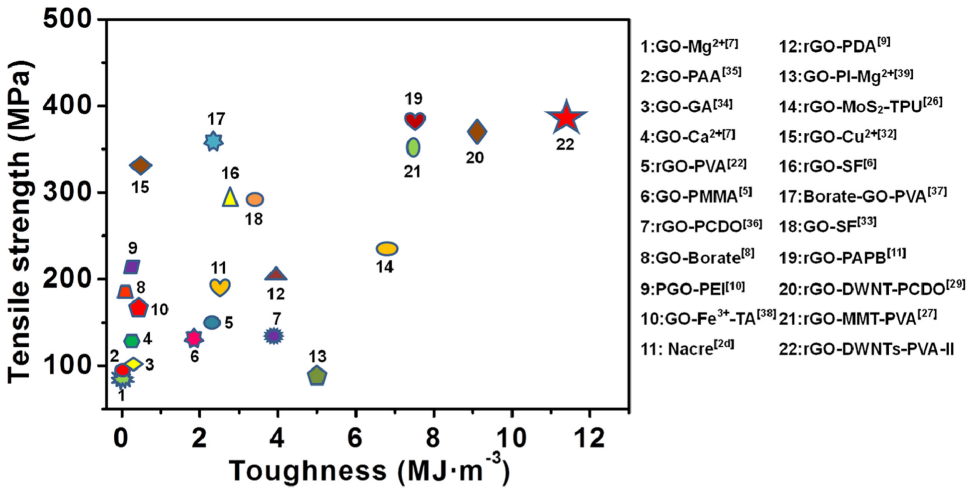

Figure 3. In comparison with other layered composites and natural nacre, our ternary rGO-DWNTs-PVA nanocomposites possesses integrated tensile strength and toughness.

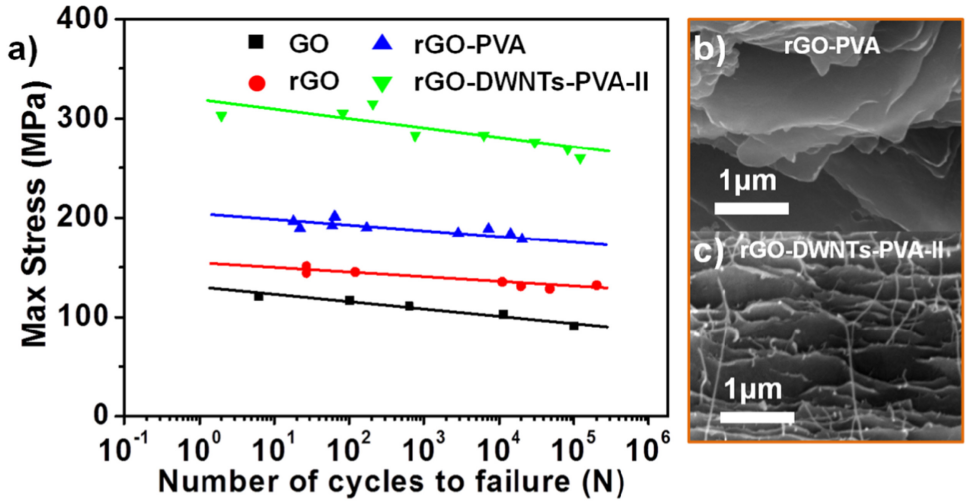

Figure 4. (a) S-N curves in pure tension pattern for pure GO film, rGO film, binary rGO-PVA and ternary rGO-DWNTs-PVA-II nanocomposites, showing outstanding fatigue performance. (b) and (c) Fracture morphology of binary rGO-PVA nanocomposite and ternary rGO-DWNTs-PVA-II nanocomposite after the fatigue testing more than 100 000 cycles, exhibits relatively orderly structure.

rGO-DWNTs-PVA-II nanocomposites, the crack deflection of 2D rGO nanosheets could inhibit the crack propagation and increase the fracture superficial area during crack propagation, while the crack bridging and a frictional pull-out of 1D DWNTs [40] also suppress crack propagation, as a consequence, the mechanical interlocking and adhesion between the building blocks and the PVA matrix are improved [41]. The crack mechanics model reduces the fatigue crack propagation rate and simultaneously increases more energy dissipation [42], resulting in higher tensile strength and toughness for our ternary artificial nacre [42, 43], and thus dramatically increasing fatigue life. In comparison with conventional binary rGO-PVA nanocomposites and other graphene-based artificial nacre [27–29], this kind of ternary bioinspired nanocomposite shows outstanding fatigue resistance performance. After millions of cycles of fatigue testing, the binary rGO-PVA nanocomposites (figure 4(b)) and ternary rGO-DWNTs-PVA-II nanocomposites (figure 4(c)) show much orderly fracture morphologies than that of static mechanical testing and the DWNTs are curled much more, further confirming the synergistic toughening effect of the two building blocks. This work indicates that the potential of significantly extend the fatigue life for bioinspired materials could be widely used in engineering device systems [43].

With the purpose of quantifying the synergy effect for continuously improving the mechanical properties in ternary rGO-DWNTs-PVA nanocomposites, Prasad [44] proposed the synergy percentage (S), which is

modified as follows:

$$S = \frac{2\sigma_{hyb} - (\sigma_{DWNTs\text{-}PVA} + \sigma_{GO\text{-}PVA})}{\sigma_{DWNTs\text{-}PVA} + \sigma_{GO\text{-}PVA}} \times 100,$$

where σ_{hyb}, $\sigma_{GO\text{-}PVA}$ and $\sigma_{DWNTs\text{-}PVA}$ represent the tensile strength of ternary GO-DWNTs-PVA nanocomposites, binary GO-PVA and DWNTs-PVA nanocomposites, respectively. The corresponding synergy percentages in tensile strength for ternary GO-DWNTs-PVA and rGO-DWNTs-PVA nanocomposites of different duilding blocks contents are summarized in table S3. It is obvious that the ternary GO-DWNTs-PVA-II and rGO-DWNTs-PVA-II nanocomposites have higher synergy percentage than other nanocomposites. The results indicate that the ternary artificial nacre with optimum mechanical properties possesses the maximum synergy percentage, showing favorable synergistic toughening effect of building blocks.

In summary, inspired by natural nacre, we successfully fabricated the ternary rGO-DWNTs-PVA bio-inspired nanocomposites with integrated tensile strength and toughness througth the synergistic toughening of 2D rGO nanosheets and 1D DWNTs. With assistance of PVA molecules, the ternary artificial nacre also shows excellent fatigue performance. This unique ternary artificial nacre could have great promising potential applications in aerospace, flexible electronics devices and other fields. This bioinspired strategy also provides a promising avenue for preparing robust bioinspired graphene-based composites with integration of strong and tough properties in the future.

Acknowledgments

This work was supported by the Excellent Young Scientist Foundation of NSFC (51522301), the National Natural Science Foundation of China (21273017, 51103004), the Program for New Century Excellent Talents in University (NCET-12-0034), the Fok Ying-Tong Education Foundation (141045), the Open Project of Beijing National Laboratory for Molecular Sciences, the 111 Project (B14009), the Aeronautical Science Foundation of China (20145251035, 2015ZF21009), the State Key Laboratory for Modification of Chemical Fibers and Polymer Materials, Donghua University (LK1508), and the Fundamental Research Funds for the Central Universities (YWF-15-HHXY-001, and YWF-16-BJ-J-09).

References

[1] Currey J D 1977 *Proc. R. Soc. Lond., Ser. B: Biol. Sci.* **196** 443
Li X Q and Zeng H C 2012 *Adv. Mater.* **24** 6277
[2] Yao H B, Fang H Y, Wang X H and Yu S H 2011 *Chem. Soc. Rev.* **40** 3764
Wang J, Cheng Q and Tang Z 2012 *Chem. Soc. Rev.* **41** 1111
Cheng Q, Jiang L and Tang Z 2014 *Acc. Chem. Res.* **47** 1256
Meyers M A, McKittrick J and Chen P-Y 2013 *Science* **339** 773
[3] Zhang Y, Gong S, Zhang Q, Ming P, Wan S, Peng J, Jiang L and Cheng Q 2016 *Chem. Soc. Rev.* **45** 2378
[4] Liu Y, Xie B and Xu Z 2011 *J. Mater. Chem.* **21** 6707
[5] Putz K W, Compton O C, Palmeri M J, Nguyen S T and Brinson L C 2010 *Adv. Funct. Mater.* **20** 3322
[6] Hu K, Tolentino L S, Kulkarni D D, Ye C, Kumar S and Tsukruk V V 2013 *Angew. Chem., Int. Ed.* **52** 13784
[7] Park S, Lee K-S, Bozoklu G, Cai W, Nguyen S T and Ruoff R S 2008 *ACS Nano* **2** 572
[8] An Z, Compton O C, Putz K W, Brinson L C and Nguyen S T 2011 *Adv. Mater.* **23** 3842
[9] Cui W, Li M, Liu J, Wang B, Zhang C, Jiang L and Cheng Q 2014 *ACS Nano* **8** 9511
[10] Tian Y, Cao Y, Wang Y, Yang W and Feng J 2013 *Adv. Mater.* **25** 2980
[11] Zhang M, Huang L, Chen J, Li C and Shi G 2014 *Adv. Mater.* **26** 7588
[12] Coleman J N *et al* 2011 *Science* **331** 568
[13] Podsiadlo P *et al* 2007 *Science* **318** 80
[14] Munch E, Launey M E, Alsem D H, Saiz E, Tomsia A P and Ritchie R O 2008 *Science* **322** 1516
Bonderer L J, Studart A R and Gauckler L J 2008 *Science* **319** 1069
[15] Yao H B, Fang H Y, Tan Z H, Wu L H and Yu S H 2010 *Angew. Chem.* **49** 2140
[16] Chen I W, Liang R, Zhao H, Wang B and Zhang C 2011 *Nanotechnology* **22** 485708
Cranford S W, Brommer D B and Buehler M J 2012 *Nanoscale* **4** 7797
[17] Oner Ekiz O, Dericioglu A F and Kakisawa H 2009 *Mater. Sci. Eng.* C **29** 2050
[18] Liu Y T, Tan Z, Xie X M, Wang Z F and Ye X Y 2013 *Chem. Asian J.* **8** 817
[19] Li D and Kaner R B 2008 *Science* **320** 1170
Huang X, Qi X, Boey F and Zhang H 2012 *Chem. Soc. Rev.* **41** 666
Huang X, Zeng Z, Fan Z, Liu J and Zhang H 2012 *Adv. Mater.* **24** 5979
[20] Kim J Y, Kim T, Suk J W, Chou H, Jang J H, Lee J H, Kholmanov I N, Akinwande D and Ruoff R S 2014 *Small* **10** 3405
[21] Dikin D A, Stankovich S, Zimney E J, Piner R D, Dommett G H, Evmenenko G, Nguyen S T and Ruoff R S 2007 *Nature* **448** 457
[22] Li Y Q, Yu T, Yang T Y, Zheng L X and Liao K 2012 *Adv. Mater.* **24** 3426
[23] Cheng Q, Duan J, Zhang Q and Jiang L 2015 *ACS Nano* **9** 2231
[24] Li Y, Yang T, Yu T, Zheng L and Liao K 2011 *J. Mater. Chem.* **21** 10844
[25] Zhang C, Huang S, Tjiu W W, Fan W and Liu T 2012 *J. Mater. Chem.* **22** 2427
[26] Wan S, Li Y, Peng J, Hu H, Cheng Q and Jiang L 2015 *ACS Nano* **9** 708

[27] Ming P, Song Z, Gong S, Zhang Y, Duan J, Zhang Q, Jiang L and Cheng Q 2015 *J. Mater. Chem.* A **3** 21194
[28] Wang J, Cheng Q, Lin L and Jiang L 2014 *ACS Nano* **8** 2739
[29] Gong S, Cui W, Zhang Q, Cao A, Jiang L and Cheng Q 2015 *ACS Nano* **9** 11568
[30] Wegst U G, Bai H, Saiz E, Tomsia A P and Ritchie R O 2015 *Nat. Mater.* **14** 23
[31] Chen J *et al* 2015 *Carbon* **94** 845
Compton O C, Cranford S W, Putz K W, An Z, Brinson L C, Buehler M J and Nguyen S T 2012 *ACS Nano* **6** 2008
[32] Hwang J, Yoon T, Jin S H, Lee J, Kim T S, Hong S H and Jeon S 2013 *Adv. Mater.* **25** 6724
[33] Yin Y, Hu K, Grant A M, Zhang Y and Tsukruk V V 2015 *Langmuir* **31** 10859
[34] Gao Y, Liu L-Q, Zu S-Z, Peng K, Zhou D, Han B-H and Zhang Z 2011 *ACS Nano* **5** 2134
[35] Park S, Dikin D A, Nguyen S T and Ruoff R S 2009 *J. Phys. Chem.* C **113** 15801
[36] Cheng Q, Wu M, Li M, Jiang L and Tang Z 2013 *Angew. Chem., Int. Ed.* **52** 3750
[37] Liu L, Gao Y, Liu Q, Kuang J, Zhou D, Ju S, Han B and Zhang Z 2013 *Small* **9** 2466
[38] Liu R-Y and Xu A-W 2014 *RSC Adv.* **4** 40390
[39] Kong J-Y, Choi M-C, Kim G Y, Park J J, Selvaraj M, Han M and Ha C-S 2012 *Eur. Polym. J.* **48** 1394
[40] Zhang W, Picu R C and Koratkar N 2007 *Appl. Phys. Lett.* **91** 193109
Zhang W, Picu R C and Koratkar N 2008 *Nanotechnology* **19** 285709
[41] Yavari F, Rafiee M A, Rafiee J, Yu Z Z and Koratkar N 2010 *ACS Appl. Mater. Inter.* **2** 2738
Yavari F, Chen L, Zandiatashbar A, Yu Z and Koratkar N 2012 *J. Nanosci. Nanotechnol.* **12** 3165
[42] Zandiatashbar A, Picu R C and Koratkar N 2012 *J. Eng. Mater. Technol.* **134** 031011
Rafiee M A, Rafiee J, Srivastava I, Wang Z, Song H, Yu Z Z and Koratkar N 2010 *Small* **6** 179
[43] Chow P K, Eksik O and Koratkar N 2014 *Part. Part. Syst. Charact.* **31** 337
Zhang W, Srivastava I, Zhu Y F, Picu C R and Koratkar N A 2009 *Small* **5** 1403
[44] Prasad K E, Das B, Maitra U, Ramamurty U and Rao C N 2009 *Proc. Natl Acad. Sci. USA* **106** 13186